Meshless Local Petrov-Galerkin Micromechanical Analysis of Periodic Composites Including Shear Loadings

Thi D. Dang[1] and Bhavani V. Sankar[2]

Abstract: In this paper the meshless local Petrov-Galerkin (MLPG) method is used in the micromechanical analysis of a unidirectional fiber composite. The methods have been extended to include shear loadings, thus permitting a more complete micromechanical analysis of the composite subjected to combined loading states. The MLPG formulation is presented for the analysis of the representative volume element (RVE) of the periodic composite containing material discontinuities. Periodic boundary conditions are imposed between opposite faces of the RVE. The treatment of periodic boundary conditions in the MLPG method is handled by using the multipoint constraint technique. Examples are presented to illustrate the effectiveness of the current model, and it is validated by comparing the results with available analytical and numerical results. The current method shows a great potential in applications to composite material analysis, especially in micromechanics of composites, wherein the complexities of meshing can be avoided.

Keyword: Composite Materials; Elastic Constants; Meshless Local Petrov-Galerkin (MLPG) Method; Micromechanical Analysis; Periodic Boundary Conditions

1 Introduction

For years there has been an interest in developing efficient methods for the prediction of effective material properties of fiber reinforced composite materials (Ishikawa and Chou, 1982; Chou and Ishikawa, 1983; Christensen, 1990; Whitcomb, 1991; Naik, 1994; Marrey and Sankar, 1995; Poe et al, 1997; Cox and Flanagan, 1997; Peng and Cao, 2000). The methods developed include empirical models, finite element based micromechanics, analytical models and experimental techniques. Due to the immense variety of available composite materials and possible fiber architecture, it is impractical and very time consuming to characterize them by experimental approach. Analytical models, on the other hand, cannot deal with complex microstructures. Though the finite element method is effective in predicting material properties (Yi at al, 1998; Takano at al, 1999), the huge computational cost limits its application in modeling complex microstructures such as in textile composites. Furthermore, the finite element based micromechanical models are satisfactory for stiffness prediction because stiffness properties are based on volume averaging of stresses and strains in the representative volume element of the composite. The approximation involved in the FE meshing does not affect the results significantly. However, modeling the damage, especially progressive damage, requires accurate description of the stress field in different phases and requires a very fine mesh as reported by Marrey and Sankar (1995) and Zhu et al. (1998). The FEM-based micromechanical models have been successfully employed in predicting thermoelastic constants of many composites materials; their use for strength prediction under multiaxial loading conditions is not practical (Zhu et al, 1998).

In the development of advanced composite materials, especially textile composites such as braided and woven composites, one of the major technical barriers is the finite element mesh generation

---

[1] Present address: Department of Aerospace & Ocean Engineering, Virginia Tech, VA 24061.

[2] Department of Mechanical and Aerospace Engineering, University of Florida, Gainesville, FL 32611- 6250, USA. Ebaugh Professor and corresponding author, Tel.: +1 352 392 6749, Fax: +1 352 392 7303. E-mail address: sankar@ufl.edu (B.V. Sankar)

(Marrey and Sankar, 1995). For composite materials with complex yarn architectures, the meshing of individual yarns in the unit-cell is quite simple as they are simply connected; however the meshing of interstitial region between matrix phases and individual yarns is much more difficult. The region is multiply connected, and meshes in different phases may not be compatible (Kim and Swan, 2003). It is difficult to get a suitable mesh in which opposite faces of the RVE have identical nodes so that periodic boundary conditions can be implemented using multi-point constraints.

We expect that the tediousness and inaccuracies involved in mesh generation and hence inaccuracies in the results can be avoided by using a new class of meshless techniques that do not require a mesh to discretize the problem. One such technique is the meshless local Petrov-Galerkin method (MLPG) recently developed by Atluri (2004). The MLPG approach proposed by Atluri and Zhu (1998a, 1998b) is one of the several meshless schemes. The main advantage of this method compared to other meshless methods is that no background mesh is used to evaluate various integrals appearing in the local weak formulation of the problem. Therefore, this method is a truly meshless approach in terms of both interpolation of variables and weighted-integration of the equilibrium equations. The meshless methods have been recently improved and demonstrated to be efficient in solving a variety of problems, in 2-D and 3-D elasticity problems (Atluri et al., 1999, 2000, 2002; Raju and Chen, 2001; Raju and Phillips, 2003; Nie, Atluri and Zuo, 2006; Atluri , Liu, and Han, 2006a, 2006b); plate and shell problems (Li et al, 2005; Sladek et al, 2006a; Jarak, Soric and Hoster, 2007); multiscale problems (Shen and Atluri, 2004; Shen and Atluri, 2005); nonlinear problems with large deformations and rotations (Han, Rajendran and Atluri, 2005); dynamic and fracture problems (Ching and Batra, 2001; Batra and Ching 2002; Han and Atluri, 2004; Sladek et al, 2005; Andreaus, Batra and Porfiri, 2005; Gao, K. Liu and Y. Liu; 2006); heat and thermoelastic Analysis (Sladek et al, 2006b; Ching and Chen, 2006; Sladek et al,

2007); solving PDEs and ODEs (Atluri and Shen, 2005; Mai-Cao and Tran-Cong, 2005); impact, penetration and perforation problems (Han et al, 2006; Liu et al, 2006); non-isothermal fluid flow problems(Arefmanesh, Najafi and Abdi, 2008).

In this study the MLPG method is applied to micromechanics of composites. A major drawback in applying meshless methods to problems of inhomogeneous materials is the treatment of material discontinuity at the interface. The high-order continuity of the moving least squares approximation (MLS), which is at least C^1, allows for continuity of displacements and stresses throughout the sub-domain. However, the high order continuity imposes a difficulty when considering discontinuities of derivatives at the interface of inhomogeneous bodies, because the shape functions from the MLS approximations do not have the Dirac delta function properties. For the analysis of linear elastostatic problems by the element free Galerkin method (EFG), Cordes and Moran (1996) used the method of Lagrange multipliers; Krongauz and Belytschko (1998) employed a special jump function at the line or the surface of discontinuity with parameters governing the strength of discontinuity; and Cai and Zhu (2004) used the direct imposition of essential boundary and interface conditions. Whereas Cordes and Moran studied a two-dimensional elastostatic problem, Krongauz and Belytschko as well as Cai and Zhu analyzed a one-dimensional elastostatic problem, all based on EFG method. Batra et al. (2004) also used the MLPG method to analyze heat conduction in which the continuity of the normal component of heat flux at the interface between two materials is satisfied either by the method of Lagrange multipliers or by using a jump function. Li et al. (2003) introduced a method for the treatment of material discontinuity by combining the MLPG-5 method and the MLPG-2 method. The MLPG-5 method is used inside the homogenous domain; the MLPG-2 method is used only at the interface. The weak form of the MLPG-2 method uses the Dirac delta function on the nodal location. Another main drawback in applying the MLPG method to the micromechanical analysis of composite materials is the treatment of peri-

odic boundary conditions. In the finite element method one can use a penalty formulation or Lagrange multipliers to enforce the periodic boundary conditions. However, there are some difficulties in using this approach in the MLPG method due to its nature of using local weak forms over overlapping sub-domains.

In the current paper the meshless local Petrov-Galerkin (MLPG) micromechanical analysis has been presented and extended to include shear loadings, both out of plane and in-plane shear, thus permitting a more complete micromechanical analysis of composites. For the treatment of material discontinuity at the interface between different phases of the composite, we used the technique of direct imposition as shown by the authors (Dang and Sankar, 2005, 2007), in which the different phases of the composite are considered as distinct homogeneous bodies. The MLS approximation is used separately within each of the homogeneous domains. The actual displacements are to be computed at the nodes on the material interface. After that, conditions of continuity of displacements at the interface are directly enforced as in the FE method. For the treatment of periodic boundary conditions, we propose an algorithm using the multipoint constraints to handle the periodic boundary conditions in the MLPG method.

Composites are periodic structures, if a representative volume element or a unit cell that repeats itself throughout the volume of the composite can be identified. The unit cell can be considered as the smallest possible building block for the composites such that the composite can be constructed from spatially translated copies of it, without the use of rotations or reflections. The response of the composites to external loads can then be computed by analyzing the behavior of a single unit cell with suitable boundary conditions.

Appropriate boundary conditions of the unit cells have been derived from the symmetry considerations for micromechanical analysis by many authors (Chou and Ko, 1989; Marrey and Sankar, 1995; Cox and Flanagan, 1997; Li, 1999; Whitcomb, Chapman and Tang, 2000; Tang and Whitcomb, 2003). Most of the authors implemented periodic boundary conditions using multipoint constraints in commercial finite element software. In general there are three methods used to implement multipoint constraints in finite element codes (Shephard, 1984; Mechnik, 1991; Farhat, Lacour and Rixen, 1998; Miyamura, 2007): (1) the master-slave nodes method, (2) the penalty method and (3) the Lagrange multiplier method. According to our experience, it is difficult to use the last two methods to enforce the multipoint constraints in the MLPG method due to its nature of using local weak forms over overlapping sub-domains. We can use these methods to enforce the essential or natural boundary conditions on the same boundary, but to impose the displacement or stress constraints (multipoint constraints) on different boundaries in the MLPG in which test and trial functions are chosen from different functional spaces is very difficult. Because the shape functions from the MLS approximations do not have the Dirac delta function properties, the implementation of the multipoint constraints in the MLPG methods is more complicated than that in the finite element methods.

In our previous work (Dang and Sankar, 2007), we use the micromechanical model to predict the stiffness properties of composites for cases $\varepsilon_{11}^{M} = 1$, $\varepsilon_{22}^{M} = 1$, $\varepsilon_{33}^{M} = 1$ only (see Table 1). For these cases, because of load and geometry symmetry of the unit cell, only one quadrant of the unit cell need be considered to describe the behavior of the unit cell (see Figure 1). Therefore the periodic boundary conditions were replaced by simple boundary conditions, and the implementation of the periodic boundary conditions using multipoint constraints were not carried out in that paper (Dang and Sankar, 2007).

In the current study we developed the micromechanical model using the MLPG method to predict the stiffness properties of composites for six cases of the macro-strains. In this problem, the treatment of periodic boundary conditions is required for the case of shear test in the $x_1 - x_2$ plane corresponding to the imposed macro-strain $\gamma_{12}^{M} = 1$ on the RVE. The quadrant of the RVE in Figure 1b is not suitable for this analysis. Therefore we use the full model of the RVE as shown

in Figure 4 to analyze the problem.

The paper is organized as follows. In Section 2, the RVE analysis, constitutive relations and periodic boundary conditions are presented. We provide the MLPG formulation for modeling the RVE of a unidirectional fiber composite corresponding to six linearly independent deformations imposed on the RVE. Also in this section, the treatment of periodic boundary conditions is presented in detail. The computation and discussion of results are given in Section 3. Conclusions are summarized in Section 4.

2 Theory of the problem

2.1 RVE analysis for three-dimensional elastic constants

The micromechanical analysis of a fiber composite is performed by analyzing the RVE of the composite using the MLPG method. We assume that uniform macro-stresses exist through the composite. It is assumed that the fibers are circular in cross section packed in a square array. Thus the representative volume element (RVE) is a square (recall we are solving a plane problem). The RVE is shown in Figure 1, where the edges of the RVE are assumed to be parallel to the coordinate axes x_1, x_2 and x_3, with RVEs repeating in all directions. The length of the square RVE is $2a$. The thickness of the RVE in the z-direction is taken as unity. The RVE analysis assumes that the composite is under a uniform state of strain on the macroscopic scale. However, the actual stresses in the fiber and the matrix within the RVE will have spatial variation. These stresses are called micro-stresses.

The macro-stresses are average stresses σ_{ij}^M required to create a given state of macro-deformations, and they can be computed from the micro-stresses σ_{ij} obtained from the MLPG method as:

$$\sigma_{ij}^M = \frac{1}{V} \int_V \sigma_{ij} dV \tag{1}$$

where V is volume of the RVE. The composite is assumed to be homogeneous and orthotropic on the macro-scale. The composite behavior is characterized by the following constitutive relation:

$$\begin{Bmatrix} \sigma_{11}^M \\ \sigma_{22}^M \\ \sigma_{33}^M \\ \tau_{23}^M \\ \tau_{31}^M \\ \tau_{12}^M \end{Bmatrix} =$$

$$\begin{bmatrix} c_{11} & c_{12} & c_{13} & c_{14} & c_{15} & c_{16} \\ & c_{22} & c_{23} & c_{24} & c_{25} & c_{26} \\ & & c_{33} & c_{34} & c_{35} & c_{36} \\ & & & c_{44} & c_{45} & c_{46} \\ & Symm. & & & c_{55} & c_{56} \\ & & & & & c_{66} \end{bmatrix} \begin{Bmatrix} \varepsilon_{11}^M \\ \varepsilon_{22}^M \\ \varepsilon_{33}^M \\ \gamma_{23}^M \\ \gamma_{31}^M \\ \gamma_{12}^M \end{Bmatrix}$$

$$\tag{2}$$

or

$$\{\sigma^M\} = [c] \{\varepsilon^M\}$$

We can calculate all stiffness constants c_{ij} corresponding to the six cases of the macro-strains, which are imposed on the boundaries of the RVE. The engineering elastic constants can be computed by the relation given below:

$$\{\varepsilon^M\} = [S] \{\sigma^M\} \tag{3}$$

where

$$[S] = [C]^{-1} =$$

$$\begin{bmatrix} \frac{1}{E_1} & -\frac{v_{21}}{E_2} & -\frac{v_{31}}{E_3} & 0 & 0 & 0 \\ -\frac{v_{12}}{E_1} & \frac{1}{E_2} & -\frac{v_{32}}{E_3} & 0 & 0 & 0 \\ -\frac{v_{13}}{E_1} & -\frac{v_{23}}{E_2} & \frac{1}{E_3} & 0 & 0 & 0 \\ 0 & 0 & 0 & \frac{1}{G_{23}} & 0 & 0 \\ 0 & 0 & 0 & 0 & \frac{1}{G_{31}} & 0 \\ 0 & 0 & 0 & 0 & 0 & \frac{1}{G_{12}} \end{bmatrix} \tag{4}$$

In the micromechanical analysis, the RVE is subjected to six linearly independent macroscopic deformations. In each deformation case, one of the six macro-strains is assumed to be non-zero and the rest of the macro-strains are set equal to zero. The six cases are: case 1: $\varepsilon_{11}^M = 1$; case 2: $\varepsilon_{22}^M = 1$; case 3: $\varepsilon_{33}^M = 1$; case 4: $\gamma_{12}^M = 1$; case 5: $\gamma_{23}^M = 1$; and case 6: $\gamma_{31}^M = 1$. The periodic boundary conditions for these six cases are shown in Table 1.
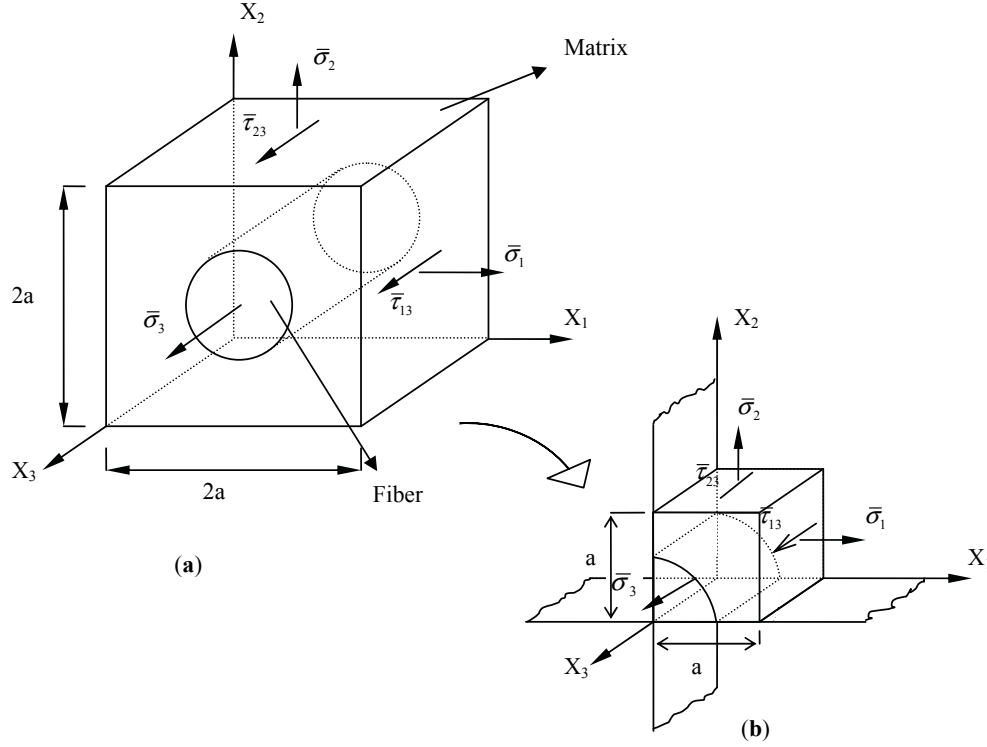
Figure 1: (a) Representative volume element RVE of a unidirectional composite; (b) Quadrant to be analyzed due to symmetry

Details of deriving the periodic boundary conditions can be found in Marrey and Sankar (1995). For all strain cases except for case 4 ($\gamma_{12}^M = 1$), (not shown in Figure 1), because of load and geometry symmetry of the RVE, only one quadrant of the RVE needs to be considered to describe its behavior. The entire RVE (Adams and Crane, 1984) is used for Case 4. Note that Case 3 $\left(\varepsilon_{33}^M = 1\right)$ is to be solved as a generalized plane strain problem, and the Cases 5 and 6 are longitudinal shear loading problems and also to be solved as special generalized plane strain problems (Adams and Doner, 1967; Gibson 1994).

Various numerical tests such as uni-axial tension in the x_1, x_2 and x_3 directions, as well as the treatment of material discontinuity at the interface have been considered by Dang and Sankar (2005, 2006). In this paper, we will extend the MLPG micromechanical analysis to include shear loadings, and focus on handling the periodic boundary conditions.

2.2 Meshless Local Petrov-Galerkin formulation for deformation in the $x_1 - x_2$ plane

Consider the general case of a composite body along with boundary conditions including periodic boundary conditions pertaining to the cases of six macro-strains. In this study, periodic boundary conditions are imposed using multi-point constraints. For simplicity, the problem has two phases separated by a single interface Γ_{intf} in the domain $\Omega = \Omega^{(1)} \cup \Omega^{(2)}$ which is bounded by $\Gamma = \Gamma_u^{(1)} \cup \Gamma_{pu}^{(1)} \cup \Gamma_t^{(1)}$ (Figure 2). The interface is defined by $n_j^{(2)}$, the unit outward normal of $\Omega^{(2)}$, along the material boundary.

The equilibrium equations in the two phases are

$$\sigma_{ij,j}^{(1)} + b_i^{(1)} = 0 \ \text{in} \ \Omega^{(1)} \tag{5}$$

$$\sigma_{ij,j}^{(2)} + b_i^{(2)} = 0 \ \text{in} \ \Omega^{(2)} \tag{6}$$

where $\sigma_{ij}^{(1)}$ and $\sigma_{ij}^{(2)}$ are the Cauchy stress tensors, $b_i^{(1)}$ and $b_i^{(2)}$ are the body forces in the two media.

Table 1: Periodic boundary conditions for the MLPG method

| Case	Constraints between left and right faces	Constraints between top and bottom faces	Out of plane strains
$\varepsilon_{11}^M = 1$	$u_1(2a,x_2) - u_1(0,x_2) = 2a$ $u_2(2a,x_2) - u_2(0,x_2) = 0$	$u_i(x_1,2a) - u_i(x_1,0) = 0$ $i = 1,2$	$\varepsilon_{33}^M = 0$, $\gamma_{31}^M = 0$, $\gamma_{23}^M = 0$
$\varepsilon_{22}^M = 1$	$u_i(2a,x_2) - u_i(0,x_2) = 0$ $i = 1,2$	$u_1(x_1,2a) - u_1(x_1,0) = 0$ $u_2(x_1,2a) - u_2(x_1,0) = 2a$	$\varepsilon_{33}^M = 0$, $\gamma_{31}^M = 0$, $\gamma_{23}^M = 0$
$\varepsilon_{33}^M = 1$	$u_i(2a,x_2) - u_i(0,x_2) = 0$ $i = 1,2$	$u_i(x_1,2a) - u_i(x_1,0) = 0$ $i = 1,2$	$\varepsilon_{33}^M = 1$, $\gamma_{31}^M = 0$, $\gamma_{23}^M = 0$
$\gamma_{12}^M = 1$	$u_1(2a,x_2) - u_1(0,x_2) = 0$ $u_2(2a,x_2) - u_2(0,x_2) = 2a$	$u_i(x_1,2a) - u_i(x_1,0) = 0$ $i = 1,2$	$\varepsilon_{33}^M = 0$, $\gamma_{31}^M = 0$, $\gamma_{23}^M = 0$
$\gamma_{23}^M = 1$	$u_3(2a,x_2) - u_3(0,x_2) = 0$	$u_3(x_1,2a) - u_3(x_1,0) = 2a$	$\varepsilon_{33}^M = 0$, $\gamma_{31}^M = 0$
$\gamma_{31}^M = 1$	$u_3(2a,x_2) - u_3(0,x_2) = 2a$	$u_3(x_1,2a) - u_3(x_1,0) = 0$	$\varepsilon_{33}^M = 0$, $\gamma_{23}^M = 0$
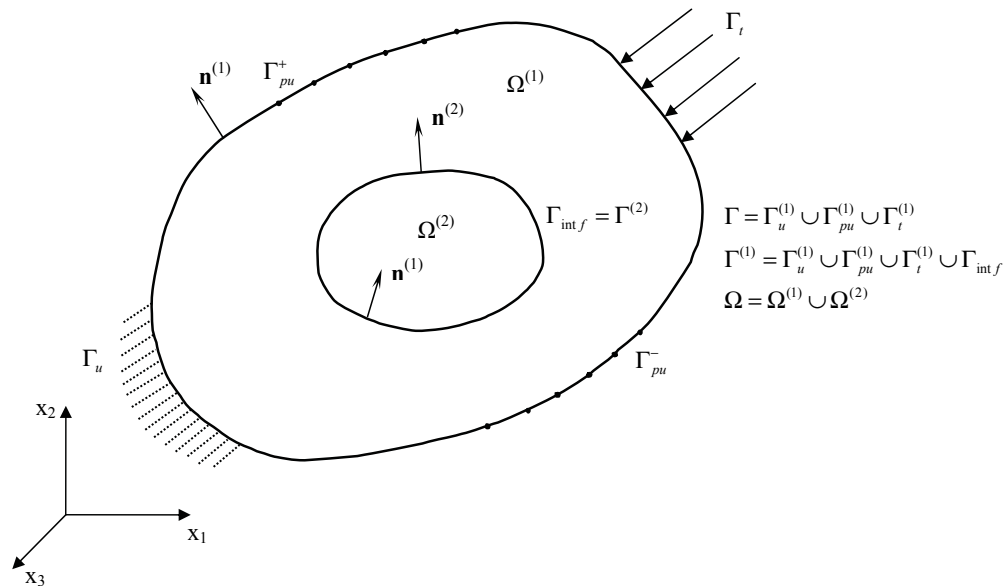
Figure 2: Illustration of an inhomogeneous body including multipoint constraints

The boundary conditions are as follows:

$$\sigma_{ij}^{(1)} n_j^{(1)} = \bar{t}_i \text{ on } \Gamma_t^{(1)} \tag{7}$$

$$u_i^{(1)} = \bar{u}_i \text{ on } \Gamma_u^{(1)} \tag{8}$$

where $\bar{t}_i$ is the prescribed traction on a surface $\Gamma_t^{(1)}$, and $\bar{u}_i$ is the prescribed displacement field $\Gamma_u^{(1)}$, and $n_j^{(1)}$ is the unit outward normal to the boundary Γ. $\Gamma_u^{(1)}$ and $\Gamma_t^{(1)}$ are complementary subsets of Γ.

The multipoint constraints for the faces Γ_{pu}^+ & Γ_{pu}^- of the body are

$$\mathbf{u}_i|_{\Gamma_{pu}^+} - \mathbf{u}_i|_{\Gamma_{pu}^-} = \mathbf{c}_i \text{ on } \Gamma_{pu}^{(1)}; \quad i = 1,\ldots,m \tag{9}$$

where m is number of nodes on the face Γ_{pu}^+ (or Γ_{pu}^-), Γ_{pu}^+ and Γ_{pu}^- are complementary subsets of

$\Gamma_{pu}^{(1)}$, and $\mathbf{c}_i$ is constant.

Continuity of tractions and displacements on the interface Γ_{intf} are given as

$$u_i^{(1)} = u_i^{(2)} \text{ on } \Gamma_{intf} \tag{10}$$

$$t_i^{(1)} = \sigma_{ij}^{(1)} n_j^{(1)} = \sigma_{ij}^{(2)} n_j^{(2)} = t_i^{(2)} \text{ on } \Gamma_{intf} \tag{11}$$

where superscripts 1 and 2 refer to variables belonging to $\Omega^{(1)}$ and $\Omega^{(2)}$, respectively.

In our study, we use the transformation approach in conjunction with the multipoint constraint technique to handle the periodic boundary conditions in equation (9); therefore we do not need to enforce the periodic boundary conditions at the variational level. The treatment of the periodic boundary conditions using the multipoint constraint technique and the transformation approach is presented in detail at the end of this section. Also in our study, we consider the inhomogeneous body as two separate homogeneous bodies, and the weak form and its discretization are presented for each of homogeneous bodies. And then we apply interface continuity conditions in equations (10-11) to reconnect the bodies via common nodes, and this is similar to the collocation method in FEM. The treatment of material discontinuity at the interface Γ_{intf} using the transformation approach and then collocation method can be found in our recent work (Dang and Sankar, 2007). In addition, we use the penalty method to enforce the essential boundary conditions in equation (8) for all cases of macro-strains imposed. In this study, the periodic boundary conditions are applied only when we use the full RVE for the case of in-plane shear $\gamma_{12}^M = 1$.

Now, we derive the weak form and its discretization for each of homogeneous media. For simplicity, we use general notations to present the weak form and its discretization below for a homogeneous body. A generalized local weak form of equations (5-8) over a local sub-domain Ω_s can be written as follows:

$$\int_{\Omega_s} (\sigma_{ij,j} + b_i) v_i d\Omega - \int_{\Gamma_u} \alpha(u_i - \overline{u}_i) v_i d\Gamma = 0 \tag{12}$$

where u_i and v_i are the trial and the test functions, respectively, and Γ_u is the part of the boundary

$\partial \Omega_s$ of Ω_s, over which essential boundary conditions are specified. In general, $\partial \Omega_s = \Gamma_s \cup L_s$ with Γ_s being the part of the local boundary located on the global boundary and L_s being the other part of the local boundary over which no boundary conditions are specified, i.e., $\Gamma_s = \partial \Omega_s \cap \Gamma$ with $\Gamma_s = \partial \Omega_s - L_s$. In equation (12), α is a penalty parameter ($\alpha \gg$ Young's modulus/Length), which is used to impose the essential boundary conditions. In this paper we choose a value of $\alpha = 10^8$. Also, the test functions v_i are chosen such that they vanish on L_s, and this can be accomplished by using the weight function w_i in the MLS approximation as also the test function v_i, but the radius r_i of the support of the weight function is replaced by the radius r_o of the local domain Ω_s.

Using integration by parts and the divergence theorem in equation (12), and after some algebraic operations, we obtain the expression in the matrix form as

$$\int_{\Omega_s} \boldsymbol{\varepsilon}_v \boldsymbol{\sigma} d\Omega + \alpha \int_{\Gamma_{su}} \mathbf{v} \mathbf{u} d\Gamma - \int_{\Gamma_{su}} \mathbf{v} t d\Gamma =$$
$$\int_{\Gamma_{st}} \mathbf{v} \bar{t} d\Gamma + \alpha \int_{\Gamma_{su}} \mathbf{v} \bar{u} d\Gamma + \int_{\Omega_s} \mathbf{v} \mathbf{b} d\Omega \tag{13}$$

In equation (13) $\boldsymbol{\varepsilon}_v$ denotes the strain matrix derived from the test functions, and $\boldsymbol{\sigma}$ is the stress vector derived from the trial functions. That is

$$\boldsymbol{\sigma} = \begin{Bmatrix} \sigma_{11} \\ \sigma_{22} \\ \sigma_{12} \end{Bmatrix}, \quad \boldsymbol{\varepsilon}_v = \begin{bmatrix} \varepsilon_{11}^{(1)} & \varepsilon_{22}^{(1)} & \gamma_{12}^{(1)} \\ \varepsilon_{11}^{(2)} & \varepsilon_{22}^{(2)} & \gamma_{12}^{(2)} \end{bmatrix} \tag{14}$$

where the superscript i denotes the ith test function. Functions $\mathbf{v, u, t}$, and $\mathbf{b}$ are defined as follows:

$$\mathbf{v} = \begin{bmatrix} v_{11} & v_{12} \\ v_{21} & v_{22} \end{bmatrix}, \quad \mathbf{u} = \begin{Bmatrix} u_1 \\ u_2 \end{Bmatrix},$$
$$\mathbf{t} = \begin{Bmatrix} t_1 \\ t_2 \end{Bmatrix}, \quad \mathbf{b} = \begin{Bmatrix} b_1 \\ b_2 \end{Bmatrix} \tag{15}$$

The two sets of test functions $\mathbf{v}$ in equation (15) should be linearly independent. The simplest choice for $\mathbf{v}$ as proposed by Atluri and Zhu (2000) is $v_{ij} = v\delta_{ij}$ or $\mathbf{v} = v\mathbf{I}$ where δ_{ij} is the Kronecker delta and $\mathbf{I}$ is the identity matrix.

As long as the union of all local sub-domains covers the global domain, equations (5-8) will be satisfied in the global domain Ω and on its boundary respectively. Using the moving least squares approximation (see Atluri and Zhu, 2000; Atluri, 2004) for the functions **u**, and substituting it into equation (13), and summing over all nodes leads to the following discretized system of linear equations:

$$
\sum_{j=1}^{n} \int_{\Omega_s} \boldsymbol{\varepsilon}_v(\mathbf{x},\mathbf{x}_i)\mathbf{DB}_j\hat{\mathbf{u}}_j d\Omega
$$

$$
+ \alpha \sum_{j=1}^{n} \int_{\Gamma_{su}} \mathbf{v}(\mathbf{x},\mathbf{x}_i)\mathbf{S}\phi_j\hat{\mathbf{u}}_j d\Gamma
$$

$$
- \sum_{j=1}^{n} \int_{\Gamma_{su}} \mathbf{v}(\mathbf{x},\mathbf{x}_i)\mathbf{NDSB}_j\hat{\mathbf{u}}_j d\Gamma
$$

$$
= \int_{\Gamma_{st}} \mathbf{v}(\mathbf{x},\mathbf{x}_i)\bar{\mathbf{t}}d\Gamma + \alpha \int_{\Gamma_{su}} \mathbf{v}(\mathbf{x},\mathbf{x}_i)\mathbf{S}\bar{\mathbf{u}}d\Gamma
$$

$$
+ \int_{\Omega_s} \mathbf{v}(\mathbf{x},\mathbf{x}_i)\mathbf{b}d\Omega \quad (16)
$$

where $\mathbf{v}(\mathbf{x},\mathbf{x}_i)$ is the value at $\mathbf{x}$ of the test function corresponding to node i, and

$$
\mathbf{N} = \begin{bmatrix} n_1 & 0 & n_2 \\ 0 & n_2 & n_1 \end{bmatrix}
$$

$$
\mathbf{B}_j = \begin{bmatrix} \phi_{j,1} & 0 \\ 0 & \phi_{j,2} \\ \phi_{j,2} & \phi_{j,1} \end{bmatrix} \qquad (17)
$$

$$
\mathbf{D} = \frac{\overline{E}}{1-\overline{v}^2} \begin{bmatrix} 1 & \overline{v} & 0 \\ \overline{v} & 1 & 0 \\ 0 & 0 & (1-\overline{v})/2 \end{bmatrix}
$$

$$
\overline{E} = \begin{cases} E & \text{for plane stress} \\ \frac{E}{(1-v^2)} & \text{for plane strain} \end{cases};
$$

$$
\overline{v} = \begin{cases} v & \text{for plane stress} \\ \frac{v}{(1-v)} & \text{for plane strain} \end{cases} \qquad (18)
$$

and

$$
\mathbf{S} = \begin{bmatrix} S_1 & 0 \\ 0 & S_2 \end{bmatrix};
$$

$$
S_i = \begin{cases} 1 & \text{if } u_i \text{ is prescribed} \\ 0 & \text{if } u_i \text{ is not prescribed on } \Gamma_u \end{cases} \qquad (19)
$$

Equation (16) can be simplified into the following system of linear algebraic equations in $\hat{u}_j$:

$$
\sum_{j=1}^{N} K_{ij}\hat{u}_j = f_t; \quad i = 1,2,...,N \qquad (20)
$$

or

$$
\mathbf{K}\hat{u} = f \qquad (21)
$$

where $\hat{\mathbf{u}}$ is the generalized fictitious displacement vector. The so-called stiffness matrix **K** and the load vector **f** are defined by:

$$
K_{ij} = \int_{\Omega_s} \boldsymbol{\varepsilon}_v(\mathbf{x},\mathbf{x}_i)\mathbf{DB}_j d\Omega + \alpha \int_{\Gamma_{su}} \mathbf{v}(\mathbf{x},\mathbf{x}_i)\mathbf{S}\phi_j d\Gamma
$$

$$
- \int_{\Gamma_{su}} \mathbf{v}(\mathbf{x},\mathbf{x}_i)\mathbf{NDB}_j\mathbf{S}d\Gamma \quad (22)
$$

$$
f_i = \int_{\Gamma_{st}} \mathbf{v}(\mathbf{x},\mathbf{x}_i)\bar{\mathbf{t}}d\Omega + \alpha \int_{\Gamma_{su}} \mathbf{v}(\mathbf{x},\mathbf{x}_i)\mathbf{S}\bar{u}d\Gamma
$$

$$
+ \int_{\Omega_s} \mathbf{v}(\mathbf{x},\mathbf{x}_i)\mathbf{b}d\Gamma \quad (23)
$$

We can use the MLPG formulation as shown above for uniaxial tension and in plane shear tests in the $x_1 - x_2$ plane with the treatment of material discontinuity and periodic boundary conditions. However, modifications have to be made for the numerical tests corresponding to the linearly independent macroscopic deformation $\varepsilon_{33}^M = 1$. The MLPG formulation for generalized plane strain problem ($\varepsilon_{33}^M = 1$) has been presented in Dang and Sankar (2005, 2006)

2.3 Out of plane shear test: special generalized plane strain problem

The case of out-of-plane shear test is a longitudinal shear problem (Adams and Doner, 1967; Gibson, 1994). The macroscopic deformation $\gamma_{13}^M = 1$ or $\gamma_{23}^M = 1$ is applied to the RVE, and for reasons mentioned above, only the quadrant of the RVE need be considered as shown in Figure 3 with the shear loading.

The problem of longitudinal shear loading is defined by a displacement field of the form:
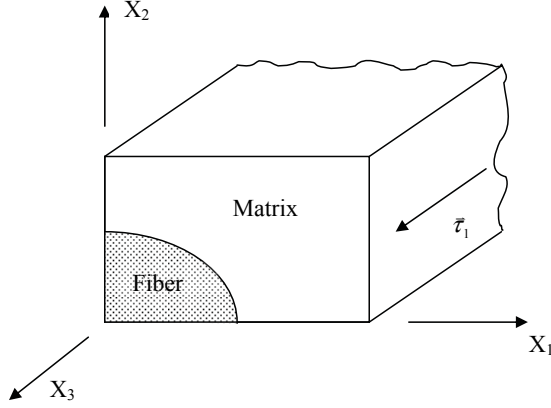
$$
u = v = 0, \quad w = w(x_1, x_2) \qquad (24)
$$

Figure 3: Longitudinal shear problem

For such a system of displacements, the only non-vanishing stress components are:

$$\tau_{31} = G_{13}\frac{\partial w}{\partial x_1}, \quad \tau_{32} = G_{23}\frac{\partial w}{\partial x_2} \tag{25}$$

where G_{13} and G_{23} are the shear moduli of the constituent materials. Thus we implicitly assume that the principal material axes of the fiber and matrix are parallel to the coordinate axes.

The assumed displacement field automatically satisfies the equilibrium equations in the x_1 and x_2 directions, while equilibrium in the x_3 direction requires that

$$\frac{\partial \tau_{31}}{\partial x_1} + \frac{\partial \tau_{32}}{\partial x_2} = 0$$

or $\tag{26}$

$$G\left(\frac{\partial^2 w}{\partial x_1^2} + \frac{\partial^2 w}{\partial x_2^2}\right) = 0$$

Using procedures similar to that given in section (2. 2), we obtain the weak form below:

$$\int_{\Omega_s}\left(\frac{\partial \tau_{31}}{\partial x_1} + \frac{\partial \tau_{32}}{\partial x_2} + b_3\right)vd\Omega - \int_{\Gamma_u}\alpha(w - \overline{w})vd\Gamma$$
$$= 0 \quad (27)$$

where $\overline{w}$ and b_3 are the prescribed displacement field and the body force, respectively in the x_3 direction. The discretized equations are derived as:

$$\sum_{j=1}^{N} K_{ij}\hat{w}_j = f_i; \quad i = 1, 2, \ldots, N \tag{28}$$

where N is the total number of nodes and $\hat{w}$ is the fictitious displacement in the x_3 direction, the stiffness and load vector are:

$$K_{ij} = \int_{\Omega_s}\boldsymbol{\varepsilon}_v(\mathbf{x}, \mathbf{x}_i)\mathbf{GB}_j d\Omega + \alpha\int_{\Gamma_{su}}v(\mathbf{x}, \mathbf{x}_i)\boldsymbol{\Phi}_j d\Gamma$$
$$- \int_{\Gamma_{su}}v(\mathbf{x}, \mathbf{x}_i)\mathbf{N}GB_j d\Gamma$$

$$f_i = \int_{\Gamma_{st}}v(\mathbf{x}, \mathbf{x}_i)\overline{t}_3 d\Omega + \alpha\int_{\Gamma_{su}}v(\mathbf{x}, \mathbf{x}_i)\overline{w}d\Gamma$$
$$+ \int_{\Omega_s}v(\mathbf{x}, \mathbf{x}_i)b_3 d\Gamma$$

$$\tag{29}$$

where $\boldsymbol{\varepsilon}_v(\mathbf{x}, \mathbf{x}_i)$ is the value of the test function corresponding to node i, evaluated at the point $\mathbf{x}$. The prescribed traction in the x_3 direction is denoted by $\overline{t}_3$, and

$$\boldsymbol{\varepsilon}_v = \{\gamma_{13} \quad \gamma_{23}\}, \quad \mathbf{N} = \{n_1 \quad n_2\},$$
$$\mathbf{B}_j = \left\{\begin{matrix}\phi_{j,1}\\ \phi_{j,2}\end{matrix}\right\},$$
$$\mathbf{G} = \begin{bmatrix}G_{13} & 0\\ 0 & G_{23}\end{bmatrix}$$

$$\tag{30}$$

2.4 Treatment of periodic boundary conditions

In the current paper, we have developed the micromechanical model using the MLPG method to predict the stiffness properties of composites for six cases of the macro-strains. In this problem, the treatment of periodic boundary conditions is required for the case of shear test in the $x_1 - x_2$ plane corresponding to the imposed macro-strain $\gamma_{12}^M = 1$ on the RVE. The quadrant of the RVE in Figure 1b is not suitable for this analysis. Therefore we use the full model of the RVE as shown in Figure 4 to analyze the problem.

The periodic boundary conditions for the RVE in this case ($\gamma_{12}^M = 1$) are given in Table 1. The periodic boundary conditions on tractions are weakly satisfied at the variational level, thus we need to only treat the periodic boundary conditions on displacements. We re-write the periodic bound-
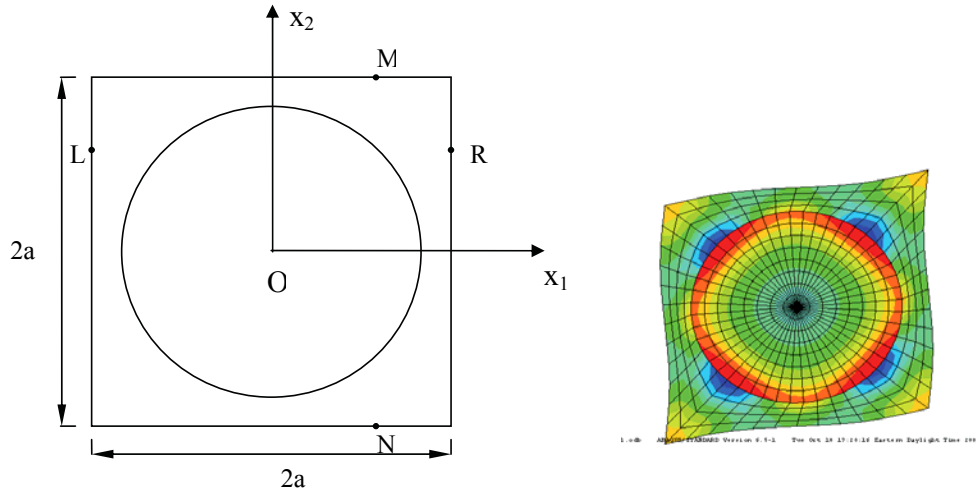
Figure 4: Illustration of periodic boundary conditions for the deformation $\gamma_{12}^M = 1$ (a) Representative volume element; (b) Periodically deformed unit cell of fiber composites

ary condition for this case as

$$
\begin{cases}
u^R - u^L = 0 \\
v^R - v^L = 2a \\
u^M - u^N = 0 \\
v^M - v^N = 0
\end{cases}
\quad \text{and} \quad
\begin{cases}
\mathbf{T}^R = -\mathbf{T}^L \\
\mathbf{T}^M = -\mathbf{T}^N
\end{cases}
\tag{31}
$$

Below is an algorithm for the treatment of periodic boundary conditions on displacements in the MLPG method using the multipoint constraint technique. Our purpose is to incorporate multipoint constraints into the equation system, which is discretized from the MLPG weak from. For clarifying our algorithm, assume that we model a body or a unit cell with 9 nodes as shown in Figure 5. Let **u** be defined as an actual displacement vector, and **û** is defined as a fictitious displacement vector.

Assume the periodic boundary condition for the opposite faces *L* & *R* of the unit cell is:

$$
\mathbf{u}_i^R - \mathbf{u}_i^L = \mathbf{c}_i, \quad i = 1, \dots, m
\tag{32}
$$

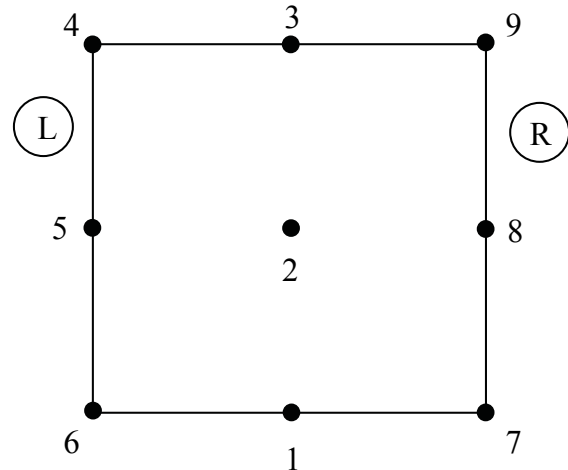where $m = 3$ is number of nodes on the face *R* (or *L*), and $\mathbf{c}_i$ are constants.

Figure 5: Illustration of a body with multipoint constraints

Expanding equation (32) we have:

$$
\begin{cases}
u_7 - u_6 = c_1 \\
v_7 - v_6 = c_2 \\
u_8 - u_5 = c_1 \\
v_8 - v_5 = c_2 \\
u_9 - u_4 = c_1 \\
v_9 - v_4 = c_2
\end{cases}
\tag{33}
$$

The periodic boundary conditions that relate to the complete degree of freedom of the unit cell $\mathbf{u}_*$ can be written in the form

where

$$
\begin{bmatrix}
0 & 0 & 0 & 0 & 0 & 0 & -1 & 0 & 0 & 0 & 0 \\
0 & 0 & 0 & 0 & 0 & 0 & 0 & -1 & 0 & 0 & 0 \\
0 & 0 & 0 & 0 & 0 & 0 & 0 & 0 & -1 & 0 & 0 \\
0 & 0 & 0 & 0 & 0 & 0 & 0 & 0 & 0 & -1 & 0 \\
0 & 0 & 0 & 0 & 0 & 0 & 0 & 0 & 0 & 0 & -1 \\
0 & 0 & 0 & 0 & 0 & 0 & 0 & 0 & 0 & 0 & 0
\end{bmatrix}
$$

$$
\begin{bmatrix}
0 & 0 & 0 & 0 & 0 & 1 & 0 \\
0 & 0 & 0 & 0 & 0 & 0 & 1 \\
0 & 0 & 0 & 1 & 0 & 0 & 0 \\
0 & 0 & 0 & 0 & 1 & 0 & 0 \\
0 & 1 & 0 & 0 & 0 & 0 & 0 \\
-1 & 0 & 1 & 0 & 0 & 0 & 0
\end{bmatrix} \{u_*\}
$$

$$
= \begin{Bmatrix}
c_1 \\ c_2 \\ c_1 \\ c_2 \\ c_1 \\ c_2
\end{Bmatrix};
$$

$$
\{u_*\}^T = \begin{bmatrix} \hat{u}_1 & \hat{v}_1 & \hat{u}_2 & \hat{v}_2 & \hat{u}_3 & \hat{v}_3 & u_4 & v_4 & u_4 & v_5 \\ u_5 & v_6 & u_7 & v_7 & u_8 & v_8 & u_9 & v_9 \end{bmatrix}
$$

(34)

or

$$[A]_{(6,18)} \{u_*\}_{(18,1)} = \{C\}_{(6,1)} \tag{35}$$

where the matrices **A** and **C** contain constants. There are more degrees of freedom in $\mathbf{u}_*$ than the constraint equations, so the matrix **A** has more columns than rows. $\mathbf{u}_*$ is partitioned as:

$$\begin{bmatrix} [A^{rL}] & [A^R] \end{bmatrix} \begin{Bmatrix} \{u_*^{rL}\} \\ \{u^R\} \end{Bmatrix} = \{C\} \tag{36}$$

where

$$\{u_*^{rL}\} = \begin{Bmatrix} \{\hat{u}^r\} \\ \{u^L\} \end{Bmatrix}$$

and

$$\{u_*\} = \begin{Bmatrix} \{u_*^{rL}\} \\ \{u^R\} \end{Bmatrix}$$

$$
[A^{rL}] =
\begin{bmatrix}
0 & 0 & 0 & 0 & 0 & 0 & -1 & 0 & 0 \\
0 & 0 & 0 & 0 & 0 & 0 & 0 & -1 & 0 \\
0 & 0 & 0 & 0 & 0 & 0 & 0 & 0 & -1 \\
0 & 0 & 0 & 0 & 0 & 0 & 0 & 0 & 0 \\
0 & 0 & 0 & 0 & 0 & 0 & 0 & 0 & 0 \\
0 & 0 & 0 & 0 & 0 & 0 & 0 & 0 & 0
\end{bmatrix}
$$

$$
\begin{bmatrix}
0 & 0 & 0 \\
0 & 0 & 0 \\
0 & 0 & 0 \\
-1 & 0 & 0 \\
0 & -1 & 0 \\
0 & 0 & -1
\end{bmatrix}_{(6,12)} \tag{37}
$$

$$
[A^R] =
\begin{bmatrix}
0 & 0 & 0 & 0 & 1 & 0 \\
0 & 0 & 0 & 0 & 0 & 1 \\
0 & 0 & 1 & 0 & 0 & 0 \\
0 & 0 & 0 & 1 & 0 & 0 \\
1 & 0 & 0 & 0 & 0 & 0 \\
0 & 1 & 0 & 0 & 0 & 0
\end{bmatrix}_{(6,6)} \tag{38}
$$

$$
\{\hat{u}^r\} = \begin{Bmatrix} \hat{u}_1 \\ \hat{v}_1 \\ \hat{u}_2 \\ \hat{v}_2 \\ \hat{u}_3 \\ \hat{v}_3 \end{Bmatrix}; \quad
\{u^L\} = \begin{Bmatrix} u_4 \\ v_4 \\ u_5 \\ v_5 \\ u_6 \\ v_6 \end{Bmatrix};
$$

$$
\{u^R\} = \begin{Bmatrix} u_7 \\ v_7 \\ u_8 \\ v_8 \\ u_9 \\ v_9 \end{Bmatrix};
$$

$$\{u_*^{rL}\} = \begin{Bmatrix} \{\hat{u}^r\} \\ \{u^L\} \end{Bmatrix}$$

$$= \begin{bmatrix} \hat{u}_1 & \hat{v}_1 & \hat{u}_2 & \hat{v}_2 & \hat{u}_3 & \hat{v}_3 & u_4 & v_4 & u_5 & v_5 & u_6 & v_6 \end{bmatrix}^T;$$

$$\{u_*\} = \begin{Bmatrix} \{u_*^{rL}\} \\ \{u^R\} \end{Bmatrix}$$

(39)

where **A** is a known $2m \times 2N$ matrix, ($m=3$, $N=9$ in the above example), $\mathbf{u}_*$ is an unknown $2N \times 1$ vector, N is total number of nodes in the unit cell. is a $(2N - 4m) \times 1$ vector of fictitious displacements of nodes which do not lie on the boundary

R & L (superscript *r* stands for the rest of displacements). is a $2m \times 1$ vector of actual displacements of nodes on the boundary*L*. is a $2m \times 1$ vector of actual displacements of nodes on the boundary *R*. $\mathbf{u}^{rL}_*$ is a $(2N-2m) \times 1$ vector. $\mathbf{A}^{rL}$ is a known $2m \times (2N - 2m)$ matrix, and $\mathbf{A}^R$ is a $2m \times 2m$ matrix.

Actually, columns of the matrix $\mathbf{A}^{rL}$ that correspond to the added fictitious displacement vector in equation (36) are zero.

Because there are as many degrees of freedom as there are independent equations of the constraint equations, the matrix $\mathbf{A}^R$ is square and nonsingular. From the first equation (36), we obtain

$$\{u^R\} = [A^{-R}] \left(\{C\} - [A^{rL}] \{u^{rL}_*\} \right) \qquad (40)$$

The complete array of degrees of freedom can be written as

$$\{u_*\} = \left\{ \begin{matrix} \{u^{rL}_*\} \\ \{u^R\} \end{matrix} \right\} = \left[\begin{matrix} [I] \\ -[A^{-R}][A^{rL}] \end{matrix} \right] \{u^{rL}_*\}$$
$$+ \left\{ \begin{matrix} \{0\} \\ [A^{-R}]\{C\} \end{matrix} \right\} \qquad (41)$$

or

$$\{u_*\} = [T]\{u^{rL}_*\} + \{Q_o\}$$
$$[T] = \left[\begin{matrix} [I] \\ -[A^{-R}][A^{rL}] \end{matrix} \right];$$
$$\{Q_o\} = \left\{ \begin{matrix} \{0\} \\ [A^{-R}]\{C\} \end{matrix} \right\} \qquad (42)$$

where **I** is a $(2N- 2m) \times (2N-2m)$ unit matrix, and the matrix **T** is a $2N \times (2N-2m)$ matrix, while $\mathbf{Q}_o$ is a $2N \times 1$ vector.

The algebraic equation system as shown in equation (21) obtained from discretizing from the MLPG weak form

$$\begin{bmatrix} k_{1,1} & k_{1,2} & ... & k_{1,18} \\ k_{2,1} & k_{2,2} & ... & k_{2,18} \\ ... & ... & ... & ... \\ k_{18,1} & k_{18,2} & ... & k_{18,18} \end{bmatrix} \{\hat{u}\}_{(18,1)} = \{f\}_{(18,1)}$$
$$\{\hat{u}\}^T = \begin{bmatrix} \hat{u}_1 & \hat{v}_1 & \hat{u}_2 & \cdots & \cdots & \hat{v}_9 \end{bmatrix}$$
$$(43)$$

or

$$[K]\{\hat{u}\} = \{f\}$$

where

$$\{\hat{u}\} = \left\{ \begin{matrix} \{\hat{u}^r\} \\ \{\hat{u}^L\} \\ \{\hat{u}^R\} \end{matrix} \right\} = \left\{ \begin{matrix} \{\hat{u}^r\} \\ \{\hat{u}^{LR}\} \end{matrix} \right\} \qquad (44)$$

$\{\hat{u}^r\}$ is defined in equation (39), and

$$\{\hat{u}^{LR}\} = \begin{bmatrix} \hat{u}_4 & \hat{v}_4 & \hat{u}_5 & \cdots & \cdots & \hat{v}_9 \end{bmatrix}^T \qquad (45)$$

Equation (43) can be rewritten in the form as

$$[K] \left\{ \begin{matrix} \{\hat{u}^r\} \\ \{\hat{u}^{LB}\} \end{matrix} \right\} = \{f\} \qquad (46)$$

The global stiffness matrix can be transformed into the form below by using the previously developed method to treat the material discontinuity at the interface with the displacement vector partitioned $\{u_*\}$ as shown in the last equation (36), in which we use the transformation formula (see Eq. (43) in Dang and Sankar, 2007), and rewrite it as

$$\{\hat{u}^{LB}\} = [\phi^{LB}]^{-1} \left[-[\phi^r]\{\hat{u}^r\} + \{u^{LB}\} \right] \qquad (47)$$

to transform equation (46) as:

$$[\tilde{K}] \left\{ \begin{matrix} \{\hat{u}^r\} \\ \{u^{LB}\} \end{matrix} \right\} = \{\tilde{f}\} \qquad (48)$$

where $[\tilde{K}]$ and $\{\tilde{f}\}$ are analogous to $[K]$ and $\{f\}$, respectively (see Eq. (45) in Dang & Sankar, 2007), and

$$\{u^{LR}\} = \begin{bmatrix} u_4 & v_4 & u_5 & \cdots & \cdots & v_9 \end{bmatrix}^T \qquad (49)$$

Obviously

$$\left\{ \begin{matrix} \{\hat{u}^r\} \\ \{u^{LB}\} \end{matrix} \right\} = \left\{ \begin{matrix} \{\hat{u}^r\} \\ \{u^L\} \\ \{u^R\} \end{matrix} \right\} = \left\{ \begin{matrix} \{u^{rL}_*\} \\ \{u^R\} \end{matrix} \right\} = \{u_*\} \quad (50)$$

So the equation (48) can be re-written as

$$[\tilde{K}]\{u_*\} = \{\tilde{f}\} \qquad (51)$$

Pre-multiplying the global equations (51) by $\mathbf{T}^T$, we hav

$$[T]^T [\tilde{K}] \{u_*\} = [T]^T \{\tilde{f}\} \qquad (52)$$

We substitute for $\{u_*\} = [T]\{u_*^{rL}\} + \{Q_o\}$ from equation (42), we obtain the reduced equation set as

$$[K^{rL}]\{u_*^{rL}\} = \{F^{rL}\} \quad (53)$$

where

$$\begin{aligned} [K^{rL}] &= [T^T][\tilde{K}][T] \\ [F^{rL}] &= [T^T]\left(\{\tilde{F}\} - [\tilde{K}]\{Q_o\}\right) \end{aligned} \quad (54)$$

After we get $\mathbf{u}_*^{rL}$ from equation (53), we can substitute it into equation (40) to obtain $\mathbf{u}^R$.

3 Results and discussions

The elastic constants such as axial and transverse modulus and Poisson's ratio have already predicted using the MLPG method. Especially, stresses at the interface and displacement comparisons have been presented in detail by the authors (Dang and Sankar; 2005, 2006). Hence, the analysis of the RVE for predicting the full three-dimensional elastic constants including shear moduli of a unidirectional E-glass/epoxy composite is presented in this section. The fiber and matrix materials of the composite were assumed isotropic. The elastic constants for the glass fiber and epoxy matrix are given in Table 2.

Table 2: Material properties of E-glass fiber and epoxy matrix

Property	E-Glass	Epoxy
Axial modulus (GPa)	73.1	3.45
Transverse modulus (GPa)	73.1	3.45
Axial Poisson's ratio	0.22	0.35
Transverse Posson's ratio	0.22	0.35
Axial shear modulus (GPa)	30.19	1.83
Volume fraction	0.503	0.497

Six numerical tests as presented in Table 1 are carried out corresponding to the linearly independent macroscopic deformations $\varepsilon_{11}^M = 1$; $\varepsilon_{22}^M = 1$; $\varepsilon_{33}^M = 1$; $\gamma_{12}^M = 1$; $\gamma_{23}^M = 1$ and $\gamma_{31}^M = 1$, which are imposed on the RVE. Except for the case of shear test in the $x_1 - x_2$ plane ($\gamma_{12}^M = 1$), because of symmetry, only one-quarter of the RVE is modeled. The boundary is represented as a square with a side dimension of 10μm ($a=10\mu$m), and the radius of fiber $R = 8\mu$m. The MLPG method with 183 nodes is used, the composite is assumed to be in a state of plane strain normal to the $x_1 - x_2$ plane. Figure 6 represents the tension tests in the x_1 and x_2 directions ($\varepsilon_{11}^M = 1$ and $\varepsilon_{22}^M = 1$) by imposing a specified uniform displacement $\overline{u}= 10\mu$m on the RVE.

For the case of shear test in the $x_1 - x_2$ plane ($\gamma_{12}^M = 1$), the full RVE as shown in Figure 7a is used, and is discretized with 577 nodes (Figure 7b), the periodic boundary conditions (equation 31) are imposed on the RVE.

Figure 8 shows the distribution of shear stresses and deformed shape of the RVE. We can see that the deformations obtained by the MLPG micromechanics are in good agreement with the FEM results as shown in Figure 8.b.

The micro-stresses are computed by the MLPG method, and then the average stresses are computed using equation (1), and finally the stiffness properties c_{ij} are computed by equation (2). From the stiffness coefficients c_{ij}, elastic constants are computed using equation (4), and they are presented in Table 3 using the notations used in composite mechanics. The elastic constants such as transverse and longitudinal modulus, Poisson's ratio computed using the current method are very close to those obtained by the Halpin-Tsai equations (Halpin and Tsai, 1969). The maximum error is 3.51% for ν_{LT}, 2.35 % for ν_{TL}, 2.27% for E_T, and the error obtained is 0.59% for E_L. Note that the Halpin-Tsai formula is not available for ν_{TT}. The current method also gives a reasonable prediction for G_{LT} and G_{TT}.

Figures 9-10 show the comparison of the computed elastic constants E_T and G_{LT} under various fiber volume fraction V_f with those from the mechanics of material approach (Kaw, 1997) and Halpin- Tsai's equation (Halpin and Tsai, 1969) as well as experimental data (Tsai, 1964; Noyes and Jones, 1968).

As shown in Figure 9, the experimental data for the transverse elastic modulus (Tsai, 1964) are quite higher compared to those obtained from the mechanics of materials approach, and are slightly
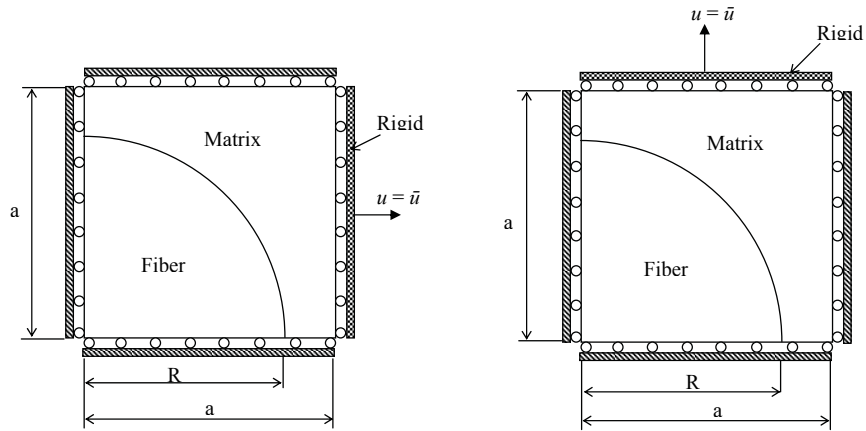
Figure 6: Tension tests in x_1 and x_2 directions ($\varepsilon_{11}^M = 1$ and $\varepsilon_{22}^M = 1$)
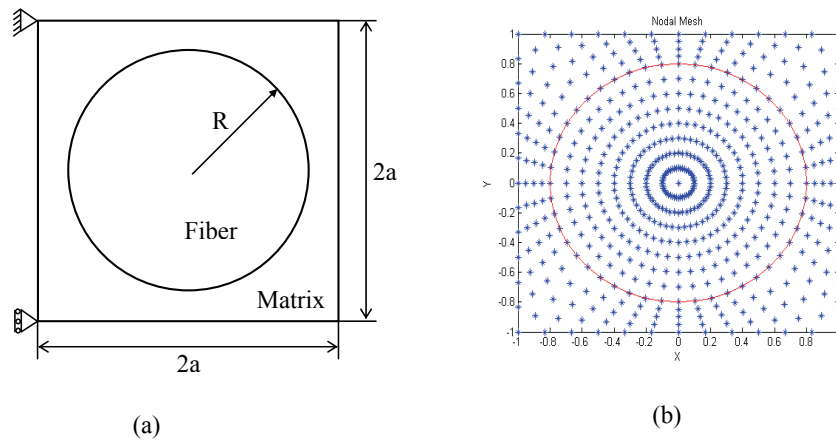

(a)

(b)

Figure 7: RVE for shear test ($\gamma_{12}^M = 1$) in the $x_1 - x_2$ plane. (a) RVE and its support; (b) nodal mesh (577 nodes)

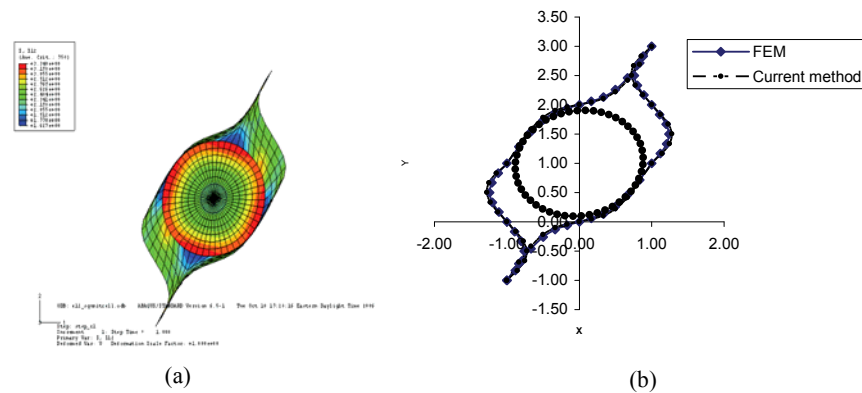FEM results as shown in Figure 8.b.

(a)

(b)

Figure 8: Periodic deformation of RVE for shear test ($\gamma_{12}^M = 1$) (a) Results from the finite element method; (b) comparison between FEM and the current MLPG method

Table 3: Comparison of elastic constants between the current method and Halpin-Tsai equations

Elastic Constants	Halpin-Tsai equations	Current MLPG Method
E_L(GPa)	38.484	38.256
E_T(GPa)	11.514	11.253
ν_{LT}	0.285	0.275
ν_{TL}	0.085	0.083
ν_{TT}	—–	0.322
G_{LT} (GPa)	4.771	5.322
G_{TT} (GPa)	3.06	2.897

lower than those predicted by the meshless local Petrov-Galerkin micromechanical analysis. The Halpin-Tsai's equation gives a good approximation due to the fact that it is a semi- analytical empirical function. The mechanics of materials approach provides a lower bound for the transverse elastic modulus.
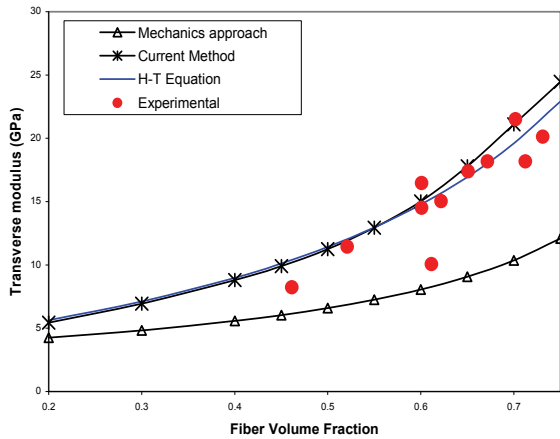

Figure 9: Comparison of transverse elastic modulus E_T of the composite

Figure 10 shows that shear modulus G_{LT} of the composite as a function of fiber volume fraction. The mechanics of materials approach underestimates the shear modulus, while the current method gives more reasonable results than the Halpin- Tsai's equation compared with the experimental data (Noyes and Jones, 1968). No experimental data of other elastic constants is available for comparison.

Table 5 shows the comparison of elastic constants obtained from the current method with those from FEM (Marrey and Sankar, 1995) and Halpin-Tsai equations for the E-glass/epoxy composite with
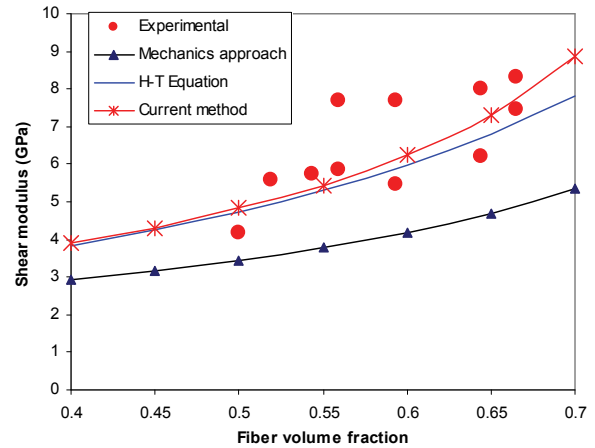

Figure 10: Comparison of shear modulus G_{LT} of the composite

Table 4: Material properties of E-glass fiber and epoxy matrix

Property	E-Glass	Epoxy
Tensile modulus (GPa)	70	3.5
Poisson's ratio	0.2	0.35
Axial shear modulus (GPa)	29.167	1.296
Volume fraction	0.6	0.4

constituent materials as shown in Table 4. We realize that the current method seems to give a better prediction than FEM for the elastic constants, especially for E_L, we can see that the current method and FEM give more reasonable result for G_{LT} than the Halpin-Tsai's equation compared with the experimental data (Noyes and Jones, 1968).

Table 5: Comparison of elastic constants by various methods including the current MLPG method

Elastic Constants	Halpin-Tsai	FEM	Current MLPG method
E_L(GPa)	43.40	43.12	43.658
E_T(GPa)	14.792	18.15	13.718
ν_{LT}	0.260	0.242	0.268
ν_{TL}	0.252	0.222	0.247
ν_{TT}	—–	0.102	0.083
G_{LT} (GPa)	4.451	5.590	5.390
G_{TT} (GPa)	3.860	3.92	3.796

4 Summary

A micromechanical analysis has been presented and extended to include shear loadings in this paper for predicting the full set of elastic constants of composite materials by modeling the RVE using the MLPG formulation.

An algorithm for the treatment of periodic boundary conditions in the MLPG method using the multipoint constraint technique has been presented for the first time. The solutions obtained from the current method are in a good agreement with FEM solutions.

The elastic constants obtained by the MLPG micromechanical analysis match well with Halpin-Tsai equations and experimental data.

The current method is a truly meshless method, wherein no elements or background cells are involved, either in the interpolation or in the integration.

The present method shows a great potential in micromechanical analysis of textile composites where the meshing of the RVE has been quite difficult.

References

Adams, D.F., Crane, D.A. (1984): Finite element micromechanical analysis of a unidirectional composite including longitudinal shear loading. *Computers & Structures* 18, 1153–1165.

Adams, D.F., Doner, D.R. (1967): Longitudinal shear loading of a unidirectional composites. *Journal of Composite Materials* 1, 4–17.

Andreaus U., Batra R.C., Porfiri M. (2005): Vibrations of cracked Euler-Bernoulli beams using meshless local Petrov-Galerkin (MLPG) method. CMES: *Computer Modeling in Engineering & Sciences* 9,111-131.

Arefmanesh A., Najafi M., Abdi H. (2008): Meshless local Petrov-Galerkin method with unity test function for non-isothermal fluid flow. CMES: *Computer Modeling in Engineering & Sciences* 25, 9-22.

Atluri S.N., Liu H.T., Han Z.D. (2006a): Meshless local Petrov-Galerkin (MLPG) mixed collocation method for elasticity problems. CMES: *Computer Modeling in Engineering & Sciences* 14, 141-152.

Atluri S.N., Liu H.T., Han Z.D. (2006b): Meshless local Petrov-Galerkin (MLPG) mixed finite difference dethod for solid mechanics. CMES: *Computer Modeling in Engineering & Sciences* 15, 1-16.

Atluri, S.N., Zhu, T. (1998a): A new meshless local Petrov-Galerkin (MLPG) approach to nonlinear problems in computational modeling and simulation. CMES: *Computer Modeling in Engineering & Sciences* 3, 187–196.

Atluri, S.N., Zhu, T. (1998b): A new meshless local Petrov-Galerkin (MLPG) approach in computational mechanics. *Computational Mechanics* 22(2), 117–127.

Atluri, S.N., Kim, H.G., Cho J.Y. (1999): A critical assessment of the truly meshless local Petrov-

Galerkin (MLPG), and local boundary integral equation (LBIE) methods. *Computational Mechanics* 24(5), 349–372.

Atluri, S.N., Zhu T.L. (2000): The meshless local Petrov- Galerkin (MLPG) approach for solving problems in elasto- statics. *Computational Mechanics* 25(2-3), 169–179.

Atluri, S.N., Shen, S. (2002): The meshless local Petrov- Galerkin (MLPG) method: A simple & less- costly alternatives to the finite element and boundary element methods. *CMES: Computer Modeling in Engineering & Sciences* 3, 11–51.

Atluri S.N., Shen S. (2005): Simulation of a 4th order ODE: Illustration of various primal & mixed MLPG methods. *CMES: Computer Modeling in Engineering & Sciences* 7, 241-268.

Atluri, S.N. (2004): The meshless method (MLPG) for domain & BIE discretizations. Tech Science Press.

Batra, R.C., Ching, H.K. (2002): Analysis of elastodynamic deformations near a crack/notch tip by the meshless local Petrov-Galerkin (MLPG) method. *CMES: Computer Modeling in Engineering & Sciences* 3, 717–730.

Batra, R.C., Porfiri, M., Spinello, D. (2004): Treatment of material discontinuity in two meshless local Petrov- Galerkin (MLPG) formulations of axisymmetric transient heat conduction. *International Journal for Numerical Methods in Engineering* 61, 2461–2479.

Belytschko, T., Krongauz, Y., Organ, D., Fleming, M., Krysl, P. (1996): Meshless Methods: An Overview and Recent Developments. *Computers Methods in Applied Mechanics and Engineering* 139, 3–47.

Cai, Y.C., Zhu, H.H. (2004): Direct imposition of essential boundary conditions and treatment of material discontinuities in the EFG method. *Computational Mechanics* 34, 330–338.

Ching, H.K., Batra, R.C. (2001): Determination of crack tip fields in linear elastostatics by the meshless local Petrov- Galerkin (MLPG) method. *CMES: Computer Modeling in Engineering & Sciences* 2, 273–289.

Ching H.K., Chen J.K. (2006): Thermomechan-ical analysis of functionally graded composites under laser heating by the MLPG method. *CMES: Computer Modeling in Engineering & Sciences* 13, 199-217.

Chou, T.W., Ishikawa, T. (1983): One dimensional micromechanical analysis of woven fabric composites. *AIAA Journal* 21, 1714–1721.

Chou, T.W and Ko, F.K. (1989): Composite Materials Series 3 – Textile Structural Composites, Elsevier Science, Amsterdam.

Christensen, R. (1990): A critical evaluation for a class of micromechanics models. *Journal of the Mechanics and Physics of Solids* 38(3), 379–404.

Cordes, L.W., Moran, B. (1996): Treatment of material discontinuity in the element- free Galerkin method. *Computers Methods in Applied Mechanics and Engineering* 139, 75–89.

Cox, B.N., Flanagan, G. (1997): Handbook of analytical methods for textile composites. NASA CR-4750.

Dang, T., Sankar, B.V. (2005): A Meshless Local Petrov-Galerkin (MLPG) Micromechanical Model for Fiber Composites. In: *Proceeding of 20th Annual Technical Conference of the American Society for Composites*, Drexel University, Philadelphia, PA.

Dang, T., Sankar, B.V. (2007): Meshless Local Petrov-Galerkin Formulation for Problems in Composite Micromechanics. *AIAA Journal* 45(4), 912–921.

Dang, T., Sankar, B.V. (2006): Meshless Local Petrov-Galerkin Micromechanical Analysis of Fiber Composites Including Axial Shear Loading. 7th *World Congress on Computational Mechanics (WCCM VII)*, Los Angeles, California, Paper Number 489.

Farhat C., Lacour C., Rixen D. (1998): Incorporation of linear multipoint constraints in substructure based iterative solvers. Part 1: A numerically scalable algorithm. *International Journal for Numerical Methods in Engineering* 43, 997–1016.

Gao G., Liu K., Liu Y. (2006): Applications of MLPG method in dynamic fracture problems. *CMES: Computer Modeling in Engineering & Sciences* 12, 181-195.

Gibson, R.F. (1994): Principles of composite material mechanics. New York, McGraw-Hill, Inc.

Halpin, J.C., Tsai, S.W. (1969): Effect of environmental factors on composite materials. *Air Force Technical Report* AFML-TR-67-243.

Han Z.D., Atluri S.N. (2004): A meshless local Petrov-Galerkin (MLPG) approach for 3-dimensional elasto-dynamics. *CMC: Computers, Materials & Continua* 1, 129-140.

Han Z.D., Rajendran A.M., Atluri S.N. (2005): Meshless local Petrov-Galerkin (MLPG) approaches for solving nonlinear problems with large deformations and rotations. *CMES: Computer Modeling in Engineering & Sciences* 10,1-12.

Han Z.D., Liu H.T., Rajendran A.M., Atluri S.N. (2006): The applications of meshless local Petrov- Galerkin (MLPG) approaches in high-speed impact, penetration and perforation problems. *CMES: Computer Modeling in Engineering & Sciences* 14, 119-128.

Ishikawa, T., Chou, T.W. (1982): Stiffness and strength behavior of woven fabric composites. *Journal of Materials Science* 17, 3211–3220.

Jarak T., Soric J., Hoster J. (2007): Analysis of shell deformation responses by the meshless local Petrov- Galerkin (MLPG) approach. *CMES: Computer Modeling in Engineering & Sciences* 18, 235-246.

Kaw, A.K. (1997): Mechanics of composite materials. New York, CRC Press.

Kim, H.J., Swan, C.C. (2003): Voxel-based meshing and unit-cell analysis of textile composites. *International Journal for Numerical Methods in Engineering* 56, 977–1006.

Krongauz, Y., Belytschko, T. (1998): EFG approximation with discontinuous derivatives. *International Journal for Numerical Methods in Engineering* 41, 1215–1233.

Li, Q., Shen, S., Han, Z.D, Atluri, S.N. (2003). Application of meshless local Petrov-Galerkin (MLPG) to problems with singularities, and material discontinuities, in 3-D elasticity. *CMES: Computer Modeling in Engineering & Sciences* 4, 571–586.

Li Q., Soric J., Jarak T., Atluri S.N. (2005): A locking-free meshless local Petrov–Galerkin formulation for thick and thin plates. *Journal of Computational Physics* 208, 116–133.

Li S. (1999): On the unit cell for micromechanical analysis of fibre-reinforced composites. *Proceedings of the Royal Society of London A*, 455, 815-838.

Liu T., Han Z.D., Rajendran A.M., Atluri S.N. (2006): Computational modeling of impact response with the RG damage model and the meshless local Petrov-Galerkin (MLPG) approaches. *CMC: Computers, Materials & Continua* 4, 43-53.

Mai-Cao L., Tran-Cong T. (2005): A meshless IRBFN-based method for transient problems. *CMES: Computer Modeling in Engineering & Sciences* 7,149-171.

Marrey, R.V., Sankar, B.V. (1995): Micromechanical models for textile structural composites. NASA CR-198229.

Mechnik, R.P. (1991): Consideration of constraints within the finite element method by means of matrix operators. *International Journal for Numerical Methods in Engineering* 31, 909–926.

Miyamura T. (2007). Incorporation of multipoint constraints into the balancing domain decomposition method and its parallel implementation. *International Journal for Numerical Methods in Engineering* 69, 326–346.

Naik, R.A. (1994): Analysis of woven and braided fabric reinforced composites. NASA CR-194930.

Nie Y.F., Atluri S.N., Zuo C.W. (2006): The optimal radius of the support of radial weights esed in moving least squares approximation. *CMES: Computer Modeling in Engineering & Sciences* 12, 137-147.

Noyes, J.V., Jones, B.H. (1968): Analytical design procedures for the strength and elastic properties of multilayer fiber composites. *Proceedings of AIAA/ASME 9th Structure Dynamics and Material Conference*, paper 68-336.

Peng, X.Q., Cao, J. (2000): Numerical determination of mechanical elastic constants of textile

composites. 15th *Annual Technical Conference of the American Society for Composites*, College Station, Texas, September, 25-27.

Poe, C.C., and Harris, C.E. (1995): Mechanics of textile composites conference. *NASA Conference Publication* 3311, Part 1 &2.

Raju, I.S., Chen, T. (2001): Meshless Petrov-Galerkin method applied to axisymmetric problems. *AIAA/ASME/ASCE/AHS/ASC Structures, Structural Dynamics, and Materials Conference*, 42nd, Seattle, WA, April 16–19.

Raju, I.S., Phillips, D.R. (2003): Local coordinate approach in meshless local Petrov- Galerkin method for beam problems. *AIAA Journal* 41, 975–978.

Sladek J., Sladek V., Wen P.H., Aliabadi M.H. (2006a): Meshless local Petrov-Galerkin (MLPG) method for shear deformable shells analysis. *CMES: Computer Modeling in Engineering & Sciences* 13, 103-117.

Sladek J., Sladek V., Zhang Ch., Tan C.L. (2006b): Meshless local Petrov-Galerkin method for linear coupled thermoelastic analysis. *CMES: Computer Modeling in Engineering & Sciences* 16, 57-68.

Sladek J., Sladek V., Zhang Ch., Solek P. (2007): Application of the MLPG to thermo piezoelectricity. *CMES: Computer Modeling in Engineering & Sciences* 22, 217-233.

Sladek J., Sladek V., Krivacek J., Zhang Ch. (2005): Meshless local Petrov-Galerkin method for stress and crack analysis in 3-D axisymmetric FGM bodies. *CMES: Computer Modeling in Engineering & Sciences* 8, 259-270.

Sankar, B.V., Marrey, R.V. (1997): Analytical method for micromechanics of textile composites. *Composites Science and Technology* 57, 703–713.

Shen, S.; Atluri, S. N. (2004): Multiscale simulation based on the meshless local Petrov-Galerkin (MLPG) method. *CMES: Computer Modeling in Engineering & Sciences* 5: 235-255.

Shen S., Atluri S.N. (2005): A tangent stiffness MLPG method for atom/continuum multiscale simulation. *CMES: Computer Modeling in Engineering & Sciences* 7, 49-67.

Shephard, M.S. (1984): Linear multipoint constraints applied via transformation as part of a direct stiffness assembly process. *International Journal for Numerical Methods in Engineering* 20, 2107-2112.

Takano, N., Uetsuji, Y., Kashiwagi, Y., Zako, M. (1999):. Hierarchical modeling of textile composite material and structures by the homogenization method. *Modelling and Simulation in Materials Science and Engineering* 7, 207-231.

Tsai, S.W. (1964): Structural behavior of composite materials. NASA CR-71.

Whitcomb, J.D. 1991: Three- dimensional stress analysis of plain weave composites. *Composite Materials Fatigue and Fracture* 3, ASTM STP 1110, 417-438.

Whitcomb, J.D., Chapman, C.D. and Tang, X. (2000): Derivation of Boundary Conditions for Micromechanics Analyses of Plain and Satin Weave Composites. *Journal of Composite Materials* 34, 724-747.

Tang X. and Whitcomb J.D. (2003): General Techniques for Exploiting Periodicity and Symmetries in Micromechanics Analysis of Textile Composites. *Journal of Composite Materials* 37, 1167-1189.

Yi, Y.M., Park, S.H., Youn, S.K. (1998): Asymptotic homogenization of viscoelastic composites with periodic microstructures. *International Journal of Solids and Structures* 35, 2039-2055.

Zhu, H., Sankar, B.V., Marrey, R.V. (1998): Evaluation of failure criteria for fiber composites using finite element micromechanics. *Journal of Composites Materials* 32, 766-782.